1990A&A...238..369M

Astron. Astrophys. 238, 369–376 (1990)

ASTRONOMY AND ASTROPHYSICS

Behaviour of highly supercritical α-effect dynamos

R. Meinel[1] **and A. Brandenburg**[2]

[1] Sternwarte Babelsberg, Rosa-Luxemburg-Strasse 17a, DDR-1591 Potsdam
[2] Observatory and Astrophysics Laboratory, University of Helsinki, Tähtitorninmäki, SF-00130 Helsinki, Finland

Received April 2; accepted June 30, 1990

Abstract. The behaviour of α^2-dynamos is discussed for highly supercritical dynamo numbers. α-quenching is assumed to be the dominant nonlinearity. Particular attention is paid to a one-dimensional reduction of the dynamo equations. For sufficiently high dynamo numbers both steady and time-dependent solutions (limit cycles) are possible. The basins of attraction of these solutions depend on the dynamo number as well as on the degree of the nonlinearity assumed. For extreme nonlinearities the limit-cycle solutions, at particular time instants (turning points), closely approach the steady solutions. In this case some noise of small but finite amplitude may cause transitions between the limit-cycle and the steady solutions. This leads to an irregular time-behaviour including nearly steady stages as well as reversals of the magnetic polarity. Implications of the different types of solutions for astrophysical dynamos are discussed.

Key words: Sun & stars: magnetic activity – hydromagnetics: mean-field dynamo – nonlinear dynamics: chaos

1. Introduction

Investigations of nonlinear mean-field dynamos have recently caused some growing interest. There are basically two directions of research in this field. One approach is concerned with various aspects of nonlinear dynamics and chaos. Usually, only simplified systems can then be studied. In the other approach one attempts to develop more realistic models for solar, stellar and other cosmic dynamos. Extensive surveys in parameter space are here prohibitively expensive in terms of computer time. In the investigations of simple "toy" systems one typically finds rich sequences of bifurcations including quasiperiodic and chaotic solutions. By a "toy" system we mean here a highly truncated set of nonlinear ordinary differential equations which has been derived from the full set of partial differential equations describing a nonlinar dynamo. A typical example of this sort is the Lorenz (1963) system of equations.

Of course, it is clear that one cannot expect such truncated toy systems to recover exactly the properties of the full dynamo equations. For example, it is not clear whether the complicated time behaviour found for simple toy systems is also typical for realistic two- or three-dimensional dynamo models. Many of the results presented so far for these more realistic models, where the original partial differential equations are solved, suggest complicated spatial structures with less complicated time behaviour.

A large variety of bifurcations to steady, periodic, and quasiperiodic solutions have been found recently also in one-dimensional $\alpha\omega$-dynamos for a wide range of dynamo numbers (Schmitt & Schüssler, 1989; Jennings, 1989; Jennings & Weiss, 1990). In two-dimensional axisymmetric $\alpha\omega$-dynamos the complexity of solutions is less, but qualitatively similar (Brandenburg et al., 1989; Jennings et al., 1990). Irregular behaviour, however, has been reported so far only for dynamos in which simplified dynamical equations for the α- or ω-effect (or both) are solved together with the induction equation (e.g. Yoshimura, 1978; Belvedere & Proctor, 1990).

In the present paper we investigate the behaviour of α^2-dynamos for very large dynamo numbers C. We begin with a general discussion of various possible types of solutions in the limit $C \to \infty$ (Sect. 2). We consider the α-quenching mechanism to be the only nonlinearity. In Sect. 3 we concentrate on a certain one-dimensional model that was introduced by Krause and Meinel (1988). This model is described by a single nonlinear partial differential equation for a complex function depending on two real variables (time and space coordinate). Most of our numerical results are obtained using a finite difference method for the integration. For testing the reliability of the numerical methods for very high dynamo numbers we also apply truncated modal expansions and a related spectral method. Finally, in Sect. 4 we discuss the relevance of our results to astrophysical dynamos.

2. General aspects

2.1. The kinematic case

Let us consider the dimensionless α^2-dynamo equation

$$\frac{\partial \boldsymbol{B}}{\partial t} = C\,\mathrm{curl}\,(\tilde{\alpha}\boldsymbol{B}) - \mathrm{curl}\,\mathrm{curl}\,\boldsymbol{B} \qquad (1)$$

(e.g. Krause & Rädler, 1980) where $\tilde{\alpha}$ represents a given spatial profile of the α parameter and C is the dynamo number.

In the case of uniform $\tilde{\alpha} \equiv 1$ in the entire space the most rapidly growing $\boldsymbol{B}$-modes are given by

Send offprint requests to: R. Meinel

© European Southern Observatory • Provided by the NASA Astrophysics Data System

1990A&A...238..369M

$$\boldsymbol{B} = \hat{\boldsymbol{B}} e^{\lambda t + \mathrm{i}\boldsymbol{k}\boldsymbol{r}}, \tag{2}$$

with

$$\lambda = \tfrac{1}{4}C^2, \quad k = \tfrac{1}{2}C, \tag{3}$$

that means these modes have a length scale of order

$$\ell = C^{-1}. \tag{4}$$

For very large dynamo numbers we obtain

$$\ell \ll 1 \quad (\text{for } C \gg 1), \tag{5}$$

and the solution (2), (3) can therefore also be used as a starting point to solve (1) for non-uniform $\tilde{\alpha}$ ($\tilde{\alpha}$ is assumed as slowly varying in comparison with ℓ) by means of a WKB method (cf. Sokoloff et al., 1983).

Thus, the response of the kinematic dynamo at highly supercritical dynamo numbers ($C \to \infty$) is characterized by an extremely short length scale of the generated magnetic field modes. This is independent of the details of $\tilde{\alpha}$ and possible boundary conditions. According to (3) all three terms in (1) become of the order of C^2 for $C \to \infty$.

Of course, these solutions are physically meaningfull only as long as ℓ is still large enough compared with the correlation length of the small-scale turbulence which is responsible for the α-effect.

2.2. The nonlinear regime

If the backreaction of the magnetic field on the motion is taken into account the growth of magnetic field modes will be limited. In the simplest cases this will lead to stationary solutions. We model the backreaction by a prescribed dependence of α on $\boldsymbol{B}$:

$$\frac{\partial \boldsymbol{B}}{\partial t} = C \operatorname{curl}[\tilde{\alpha} f(\boldsymbol{B})\boldsymbol{B}] - \operatorname{curl}\operatorname{curl}\boldsymbol{B}, \tag{6}$$

where f is a given function of $\boldsymbol{B}$ with $f = 1$ for $\boldsymbol{B} = 0$ and $f \to 0$ as $|\boldsymbol{B}| \to \infty$.

Now the response of the dynamo as $C \to \infty$ may be a stationary solution with

$$\operatorname{curl}[\tilde{\alpha} f(\boldsymbol{B})\boldsymbol{B}] = O(C^{-1}). \tag{7}$$

This can simply be achieved if $f(\boldsymbol{B}) = O(C^{-1})$, but more generally this means only

$$\tilde{\alpha} f(\boldsymbol{B})\boldsymbol{B} \to \nabla\psi \quad \text{as} \quad C \to \infty, \tag{8}$$

inside the considered integration volume. In general (8) will not be consistent with the boundary conditions. Therefore one has to expect a "boundary layer" of thickness $O(C^{-1})$ as $C \to \infty$. Thus, in contrast to the kinematic case, a short-scale spatial variation of the magnetic field will here only be found near the boundary, if at all.

An interesting additional response of the nonlinear dynamo on large dynamo numbers could be a strong time dependence of the solution leading, for example, to a limit cycle or to an irregular time behaviour. One has to expect time-scales of order of C^{-1}.

3. A nonlinear one-dimensional dynamo

To become more explicit, we now adopt a one-dimensional model which was introduced by Krause & Meinel (1988). Physically this model applies to a conducting layer of thickness unity, extending to infinity in the other two directions, surrounded by empty space. All variables are assumed to be uniform parallel to the layer and the magnetic field vectors are always oriented along the layer. By defining suitable orthogonal coordinates the two horizontal field components can be lumped together as a complex scalar field B.

3.1. The equations

The evolution of a magnetic field in this one-dimensional α^2-dynamo model is described by the nonlinear partial differential equation

$$\frac{\partial B}{\partial t} = \mathrm{i}C \frac{\partial}{\partial x}[f(B^*B)B)] + \frac{\partial^2 B}{\partial x^2} \tag{9}$$

for the complex variable $B(x,t)$ with the boundary conditions

$$B(0,t) = B(1,t) = 0. \tag{10}$$

Eq. (9) follows from the one-dimensional reduction of (6) with $\tilde{\alpha} = 1$ and f depending on $\boldsymbol{B}^2$; for details see Krause & Meinel (1988).

The steady case of the problem (9),(10) can be reduced to a single real quadrature. The steady solutions $B = B^{(n)}$ bifurcate from the trivial solution $B = 0$ at the dynamo numbers $C = C_n = 2\pi n$ ($n = 1, 2, 3, \ldots$). The trivial solution is stable for $0 \le C \le 2\pi$. Numerical stability tests reavealed that the solutions $B^{(n)}$ are unstable for $n \ge 2$. Only the first solution branch $B^{(1)}$ which bifurcates from $B = 0$ at the marginal dynamo number $C_{\mathrm{crit}} = C_1 = 2\pi$ can represent an attracting steady solution. However, in addition to this stable steady solution an attracting oscillating solution (limit cycle) was found at large dynamo numbers ($C \gtrsim 100$). This oscillating solution has no kinematic counterpart for uniform $\tilde{\alpha}$ but it becomes plausible in the light of the results of Baryshnikova et al. (1987) for non-uniform $\tilde{\alpha}$. (Note that in our nonlinear case α varies via f.) In the present paper we report on further results concerning the nonlinear steady and oscillatory solutions of Eqs. (9),(10). We first consider the case

$$f = 1 - B^*B \quad (\text{model i}), \tag{11}$$

cf. Rüdiger (1973). We also study the behaviour of the solutions for

$$f = \frac{1}{1 + (B^*B)^{\kappa}} \quad (\text{model ii}) \tag{12}$$

in dependence on the additional parameter κ ($\kappa \ge 1$). For $\kappa = 1$ this nonlinearity has been employed as a numerically convenient extension of Eq. (11) to large values of $|\boldsymbol{B}|$ (α-quenching, cf. Jepps, 1975). An interesting limiting case is given by $\kappa \to \infty$ leading to a step function

$$f = \begin{cases} 1 & \text{for } B^*B < 1 \\ 0 & \text{for } B^*B > 1 \end{cases} \quad (\text{model iii}). \tag{13}$$

This latter case has been first investigated also by Stix (1972) for another, slightly different, one-dimensional model.

© European Southern Observatory • Provided by the NASA Astrophysics Data System

1990A&A...238..369M

Note that solutions obey the following transformation properties. Suppose $B^{(1)}(t,x)$ is a solution to (9),(10) for $C = C_1$. Then also $B^{(n)}(t,x) = B^{(1)}(n^2t, nx)$ is a solution, but now for $C = C_n = nC_1$. Further, if B is a solution then also $B\exp(i\varphi_0)$ satisfies (9),(10), where φ_0 is a real constant.

3.2. Modal expansions

3.2.1. Expansion in terms of Fourier modes

The boundary conditions (10) require a Fourier-sine expansion:

$$B(x,t) = \sum_{n=1}^{\infty} A_n(t)\sin(n\pi x). \tag{14}$$

Inserting this into Eq. (9), multiplying by $\sin(m\pi x)$ and integrating over x we obtain

$$\dot{A}_m = -(m\pi)^2 A_m - 2im\pi C\int_0^1 f(B^*B)B\cos(m\pi x)dx \tag{15}$$

(a dot denotes a time derivation). In the special case (11) this leads to

$$\dot{A}_m = -(m\pi)^2 A_m + C\sum_n \gamma_{mn}A_n + C\sum_{k,l,n}\delta_{mkln}A_k^*A_lA_n \tag{16}$$

with

$$\gamma_{mn} = -2im\pi\int_0^1 \sin(n\pi x)\cos(m\pi x)dx = \begin{cases} 4i\dfrac{mn}{m^2-n^2} & \text{for } m+n \text{ odd} \\ 0 & \text{for } m+n \text{ even} \end{cases} \tag{17}$$

$$\delta_{mkln} = 2im\pi\int_0^1 \sin(k\pi x)\sin(l\pi x)\sin(n\pi x)\cos(m\pi x)dx = \begin{cases} im\left[\dfrac{k+l-n}{(k+l-n)^2-m^2} + \dfrac{k+n-l}{(k+n-l)^2-m^2} + \dfrac{l+n-k}{(l+n-k)^2-m^2} - \dfrac{k+l+n}{(k+l+n)^2-m^2}\right] & \text{for } k+l+n+m \text{ odd} \\ 0 & \text{for } k+l+n+m \text{ even} \end{cases} \tag{18}$$

A considerable simplification occurs if we assume

$$A_n = \begin{cases} a_n & \text{for } n = 1,3,5,\ldots \\ ia_n & \text{for } n = 2,4,6,\ldots \end{cases} \tag{19}$$

with real coefficients a_n. Then we obtain from (16) the real equations

$$\dot{a}_m = -(m\pi)^2 a_m + C\sum_n \Gamma_{mn}a_n + C\sum_{k,l,n}\Delta_{mkln}a_ka_la_n \tag{20}$$

with

$$\Gamma_{mn} = \begin{cases} (-1)^m\dfrac{4mn}{m^2-n^2} & \text{for } m+n \text{ odd} \\ 0 & \text{for } m+n \text{ even} \end{cases} \tag{21}$$

and $\Delta_{mkln} =$

$$= \begin{cases} (-1)^m m\left[\dfrac{k+l-n}{(k+l-n)^2-m^2} + \dfrac{k+n-l}{(k+n-l)^2-m^2} + \dfrac{l+n-k}{(l+n-k)^2-m^2} - \dfrac{k+l+n}{(k+l+n)^2-m^2}\right] \\ \quad \text{for } (k+l \text{ even and } n+m \text{ odd}) \\ 0 \quad \text{otherwise} \end{cases} \tag{22}$$

Note that the reality of Eq. (20) implies that the restriction (19) remains valid for all times if it is initially satisfied. As can be seen from Eq. (14) the restriction (19) is equivalent to the assumption that the real part of B is an even function and the imaginary part of B an odd function of x with respect the the midpoint $x = 1/2$ of the considered intervall $[0,1]$. (This assumption, of course, restricts the gauge freedom $B \to B\exp(i\varphi_0)$ and leaves only the freedom $B \to -B$.) It should be noted that all special solutions considered in this paper do indeed satisfy the assumption (19) after a suitable transformation $B \to B\exp(i\varphi_0)$.

3.2.2. Expansion in terms of eigenmodes

The general solution of Eqs. (9),(10) for $f = 1$ is given by

$$B = \sum_{n=1}^{\infty} A_n(t)B_n(x) \tag{23}$$

with $\dot{A}_n = \lambda_n A_n$,

$$\lambda_n = (C^2/4) - (n\pi)^2 \tag{24}$$

$$B_n = \exp(-iCx/2)\sin(n\pi x) \tag{25}$$

Since these eigenmodes B_n represent a complete set of orthogonal functions we may insert the representation (23) into the nonlinear equation (9) as well and obtain, in a similar way to that described in Sect. 3.2.1, the following set of ordinary differential equations for the coefficients $A_m(t)$, again using $f = 1 - B^*B$:

$$\dot{A}_m = \lambda_m A_m + C\sum_{k,l,n}\chi_{mkln}A_k^*A_lA_n \tag{26}$$

with

$$\chi_{mkln} = \begin{cases} -CP_{mkln} & \text{for } m+k+l+n \text{ even}, \\ \delta_{mkln} & \text{for } m+k+l+n \text{ odd}. \end{cases} \tag{27}$$

The δ_{mkln} are defined as in (18) and

$$P_{mkln} = \begin{cases} -1/8 \quad \text{for } (m+k+l-n)(m+k+n-l) \\ \qquad \times (m+n+l-k)(n+l+k-m) = 0, \\ h(m+k-l-n) + h(m+l-k-n) \\ \qquad + h(m+n-k-l) \quad \text{otherwise}, \end{cases} \tag{28}$$

with the auxiliary function $h(p)$ defined by

© European Southern Observatory • Provided by the NASA Astrophysics Data System

1990A&A...238..369M

$$h(p) = \begin{cases} 1/8 & \text{for } p = 0, \\ 0 & \text{for } p \neq 0. \end{cases} \tag{29}$$

Again the assumption (19) leads to a simplification:

$$\dot{a}_m = \lambda_m a_m + C \sum_{k,l,n} X_{mkln} a_k a_l a_n, \tag{30}$$

with real X_{mkln} given by

$$X_{mkln} = \begin{cases} -CP_{mkln} & \text{for } (k+l \text{ even and } m+n \text{ even}), \\ \Delta_{mkln} & \text{for } (k+l \text{ even and } m+n \text{ odd}), \\ 0 & \text{for } k+l \text{ odd}. \end{cases} \tag{31}$$

The Δ_{mkln} are defined as in (22). As can be seen from (23) and (25) the assumption (19) means again that B (after a transformation $B \to B\exp(\mathrm{i}C/4)$) has a real part which is an even function of x and an imaginary part that is odd.

3.3. Steady solutions

The steady solutions of (9),(10) are given by

$$B = k_0[CF(w) + \mathrm{i}\partial w/\partial x] \tag{32}$$

where

$$w = B^* B, \tag{33}$$

k_0 is a complex constant and the function $F(w)$ is defined by

$$\frac{dF}{dw} = f(w), \quad F(0) = 0. \tag{34}$$

The real function $w = B^*B$ has to be determined from the equation

$$(\partial w/\partial x)^2 = \rho w - C^2 F^2(w), \tag{35}$$

with

$$\rho = (k_0 k_0^*)^{-1}, \tag{36}$$

together with the boundary conditions

$$w(0) = w(1) = 0. \tag{37}$$

Eq. (35) leads to the quadrature formula

$$x(w) = \int_0^w [\rho w' - C^2 F^2(w')]^{-1/2} dw'. \tag{38}$$

The remaining boundary condition $w(1) = 0$ results, for given C, in a discrete set of possible values for the constant ρ determining the modulus of k_0. Its phase can be chosen arbitrarily. (For real k_0 the constraint (19) is satisfied.)

It can easily be checked that Eqs. (32)-(37) indeed solve the steady case of (9),(10). As an example we present the steady solutions more explicitly for f satisfying Eq. (11). (This example is even simpler than those considered by Krause and Meinel (1988).) From (11) and (34) we obtain

$$F(w) = w - \tfrac{1}{2}w^2. \tag{39}$$

The solution of (35) is then given by

$$w = a\frac{1 - \mathrm{sn}(bx + K, k)}{1 - q\,\mathrm{sn}(bx + K, k)}. \tag{40}$$

Here sn is Jacobi's function *sinus amplitudinis* with k as Legendre's modulus and

$$\left.\begin{aligned} k^2 = q^3\frac{2+q}{1+2q}, \quad K = \int_0^{\pi/2} \frac{d\psi}{(1-k^2\sin^2\psi)^{1/2}}, \\ a = \frac{2q(1+q)}{1+4q+q^2}, \quad b = C\frac{(1+2q)^{1/2}}{1+4q+q^2}, \quad 0 < q < 1. \end{aligned}\right\} \tag{41}$$

The boundary conditions (37) will be satisfied if

$$b = 4nK, \quad n = 1, 2, 3, \ldots \tag{42}$$

This leads to a relation between q and C, where $0 < q < 1$ corresponds to $2n\pi < C < \infty$, i.e., the n'th solution exists for $C > 2n\pi$.

By using Eq. (32) it is possible to derive the complete solution $B(x)$. Note that the constant ρ is given by

$$\rho = \frac{4q(1+q)^4}{(1+4q+q^2)^3} C^2. \tag{43}$$

The basic solution ($n = 1$) has its maximal value of $w = B^*B$ at $x = 1/2$:

$$w(1/2) = \frac{4q}{1+4q+q^2}. \tag{44}$$

In the limit $C \to \infty$ ($q \to 1$) we obtain $w(1/2) \to 2/3$, i.e. $f \to 1/3$. That means, the α-effect cannot be reduced to more than one third of its original value and the function f (given by (11)) remains everywhere positive.

Fig. 1 shows the $n = 1$ solution for $C = 100$. It can be seen that the condition (7) is satisfied here in the interior region via the near-constancy of B. Furthermore we indeed find "boundary layers" as described in Sect. 2.2. Table 1 shows the convergence of the results obtained by means of the truncated modal expansion of Sect. 3.2.2. The expansion in terms of eigenmodes of the linearized equations is of particular advantage in only slightly supercritical cases. For large dynamo numbers the Fourier expansion of Sect. 3.2.1 is more convenient.

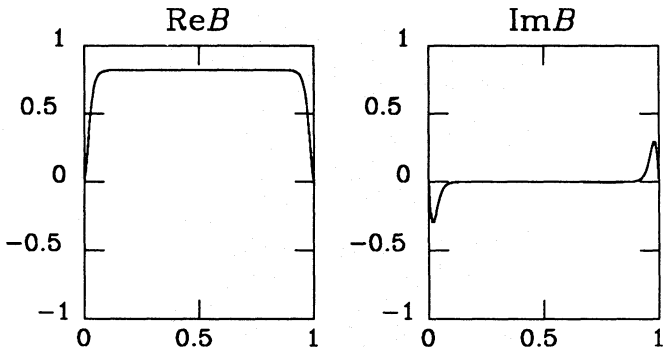

Fig. 1. The $B^{(1)}$-solution (real and imaginary part) for model (i) with $C = 100$

© European Southern Observatory • Provided by the NASA Astrophysics Data System

1990A&A...238..369M

Table 1. Energies of the steady solution in dependence on the number of eigenfunctions retained in the modal expansion of (23) for model (i)

$C\backslash N$	1	2	3	4	5	6	7	exact
10	.1009	.1297	.1242	.1238	.1239	.1239	.1239	.1239
20	.1502	.2133	.2504	.2488	.2275	.2289	.2286	.2286

3.4. Oscillatory solutions

In addition to the steady solutions determined analytically in the previous subsection we now discuss further solutions which have been computed numerically by timestepping the discretized equations.

Krause and Meinel (1988) have found an oscillatory solution of Eq. (9) for the slightly different nonlinearity $f = 1/(1+B^*B)^2$. We find similar oscillatory solutions also for the nonlinearities of models (i) and (ii). Bifurcation diagrams for the various models are shown in Fig. 2.

We have paid particular attention to the behaviour of the oscillatory solution for model (ii) with varying values of κ. It turns out that the smallest value of C ($= C^*$) for which this oscillatory solutions still exists depends on the magnitude of κ. The smallest critical values C^* are found for $\kappa \approx 4...6$. In this case the oscillatory solution is found already for C around fifty. The dependence of the period T on κ and C is displayed in Fig. 3. Clearly the period decreases monotonously with κ and C.

For large values of κ the oscillatory solution has the remarkable property that it passes very closely to the first two steady solutions $B^{(1)}$ and $B^{(2)}$ during the course of one period. This is demonstrated in Fig. 4, where ReB and ImB are plotted at two such instants (solid curves). The first two steady solutions are also plotted for comparison (dotted curves). The two instants t_1 and t_2, for which $\mathrm{Re}B(1/2,t_1) = \max(\mathrm{Re}B)$ and $\mathrm{Re}B(1/2,t_2) = 0$, are marked as vertical dotted lines on the graph ReB vs. t in Fig. 5.

The timestepping method is, of course, only capable of detecting stable solutions. Probably, the oscillatory solution continues beyond the left end (see the bifurcation diagram Fig. 2) as an unstable solution and connects somewhere with the second (unstable) steady solution branch. (Note that both steady and oscillatory secondary solutions – which prove to be unstable – can simply be constructed by applying the transformation properties discussed in Sect. 3.1.)

3.5. Extreme nonlinearities and reversals

In the limit $\kappa \to \infty$ the nonlinearity (12) degenerates to a simple step function (13). In this case (model iii) we find an irregular (chaotic) time behaviour of the solution for $C \gtrsim 40$ with magnetic field reversals. Examples of these solutions are presented in Fig. 6. It turned out that the reversals become more rarely as the number of gridpoints is increased. Also, properties of the numerical scheme adopted determine the frequency of reversals. For $N > 200$ usually reversals not longer occured. The solution is then always close to the stationary solution. However, some kind of noise is superimposed. We have found that the noise level depends on the number of gridpoints, i.e. the noise is an artefact of the numerical treatment of the extreme

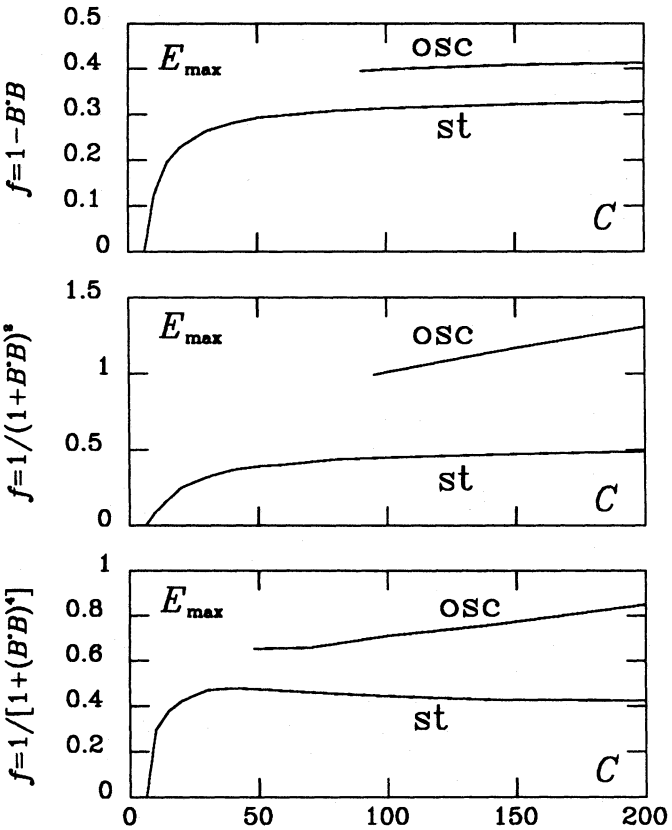

Fig. 2. Bifurcation diagram for various models. Note that in model (ii) with $\kappa = 4$ the energy of the steady solution branch is decreasing with increasing values of C when $C > 50$

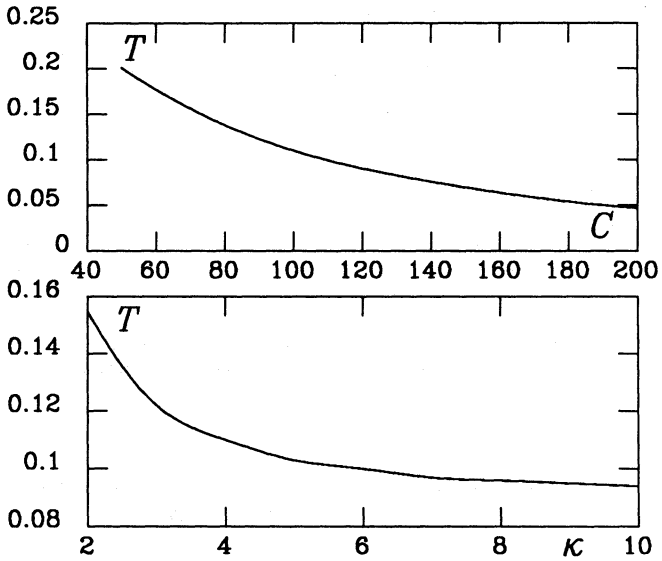

Fig. 3. The dependence of the periods T on C (for $\kappa = 4$, upper panel) and on κ (for $C = 100$, lower panel)

nonlinearity (13). We suppose that reversals can be triggered by the presence of noise.

In order to confirm this we now go back to a finite value of κ

© European Southern Observatory • Provided by the NASA Astrophysics Data System

1990A&A...238..369M

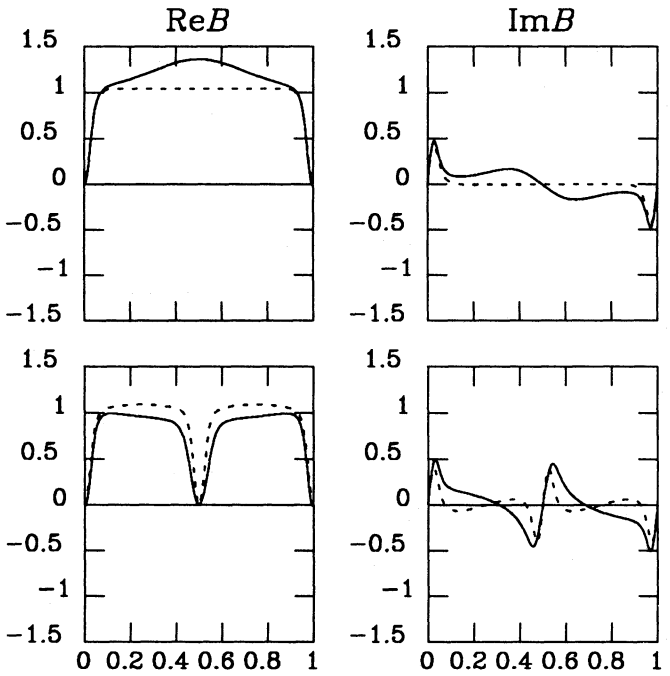

Fig. 4. Snapshots of the oscillatory solution of model (ii) for $\kappa = 4$ and $C = 50$. Solid lines show ReB and ImB at instants $t = t_1 = 0.659$ (upper panels) and $t = t_2 = 0.687$ (lower panels) for which Re$B(1/2, t_1) = \max(\mathrm{Re}B(1/2, t))$ and Re$B(1/2, t_2) = 0$. Also displayed are with broken lines the first and second steady solution (upper and lower panels, respectively). Note the close similarity between the two steady solutions and the oscillatory one at two different instants

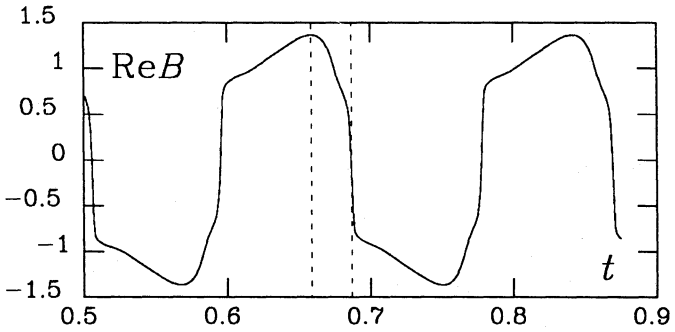

Fig. 5. Time behaviour of Re$B(1/2, t)$ for the oscillatory solution of model (ii) with $\kappa = 4$ and $C = 50$. The two vertical and dotted lines mark the instants $t = t_1$ and $t = t_2$, cf. Fig. 4

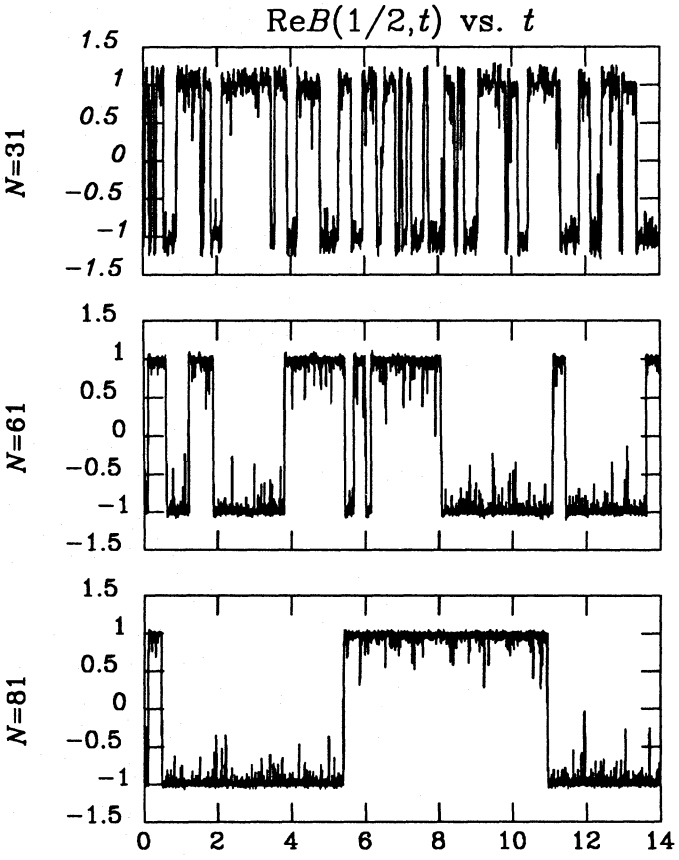

Fig. 6. Solutions for the step function profile (model iii) with $C = 50$ and for different numbers of gridpoints N. For $N = 81$ (last panel) reversals occur very rarely

($\kappa = 4$) and introduce explicitly some external stochastic driving, i.e. we modify Eq. (9) to a Langevin-type equation

$$\frac{\partial B}{\partial t} = \mathrm{i}C\frac{\partial}{\partial x}[f(B^*B)B)] + \frac{\partial^2 B}{\partial x^2} + A\,G(x)F(t). \tag{45}$$

where $G(x) = \sin \pi x + \frac{1}{2}\sin 2\pi x$ and $F(t)$ is a stochastic function defined by

$$F(t) = \sum_{k=1}^{\infty} \epsilon_k \delta(t - k\Delta t),\ t > 0. \tag{46}$$

Here ϵ_k, for each k, can take the values -1, 0, 1 with probabilities p, $1-2p$, p, respectively. We choose $\Delta t = 10^{-3}$, $p = 10^{-2}$, and the amplitude A of the perturbation to be 0.2. The results are shown in Fig. 7, where we have plotted the time series of Re$B(1/2, t)$ for the three different cases $C = 40$, 50, and 60. For $C = 40$ the time behaviour is similar to that of model (iii). Obviously, the external stochastic forcing is able to produce jumps between the steady and oscillatory solutions. In this way transitions from the steady solution of one polarity to the steady solution of the opposite polarity are induced. The reversals themselves can be interpreted approximately as parts (half periods) of the oscillatory solution. Fig. 8 shows the magnetic field evolution during one reversal in more detail.

With increasing C the oscillatory solution and with decreasing C the steady solutions dominate. (Note that for $C = 40$ the oscillatory solution does not exist as a stable one.) The higher the degree κ of the nonlinearity the more closely the oscillatory solution at its "turning points" approaches the steady $B^{(1)}$-solution of positive and negative polarities (cf. Sect. 3.4). Therefore the critical amplitude of the perturbations required to induce reversals decreases with growing κ.

We would like to stress that adding some (small) noise term in Eq. (45) is quite natural. Hoyng (1988) argues that such a term occurs as a correction to the standard mean-field equation if the Reynolds rules are not exactly satisfied in the usual two-scale approach. Thus we have here an alternative possibility of explaining random-like behaviour of mean-field dynamos, in contrast to the deterministic chaos solutions proposed previously.

© European Southern Observatory • Provided by the NASA Astrophysics Data System

1990A&A...238..369M

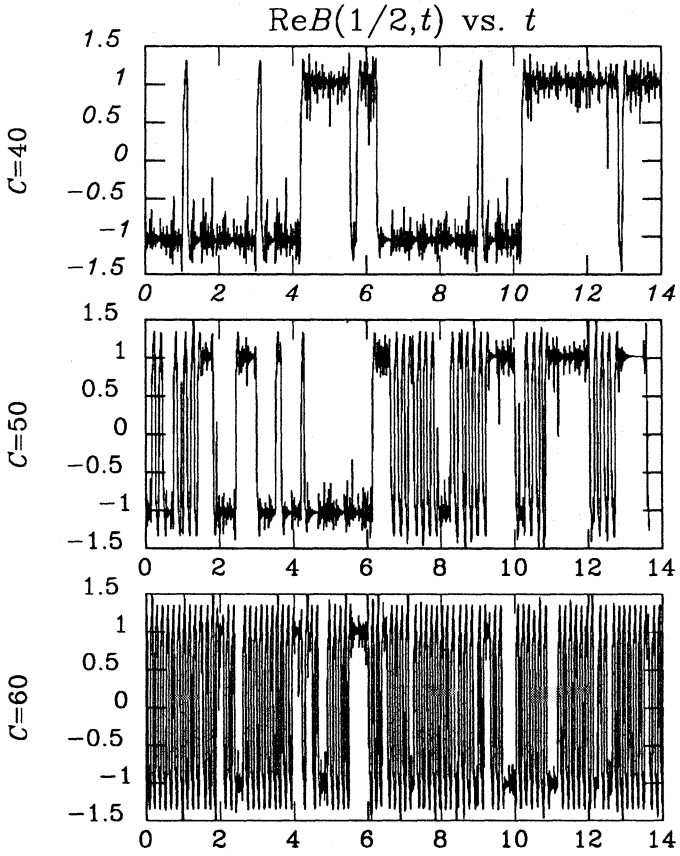

Fig. 7. Model (ii) with stochastic forcing for different values of C, $\kappa = 4$ (upper panel: $C = 40$, middle panel: $C = 50$, lower panel: $C = 60$)

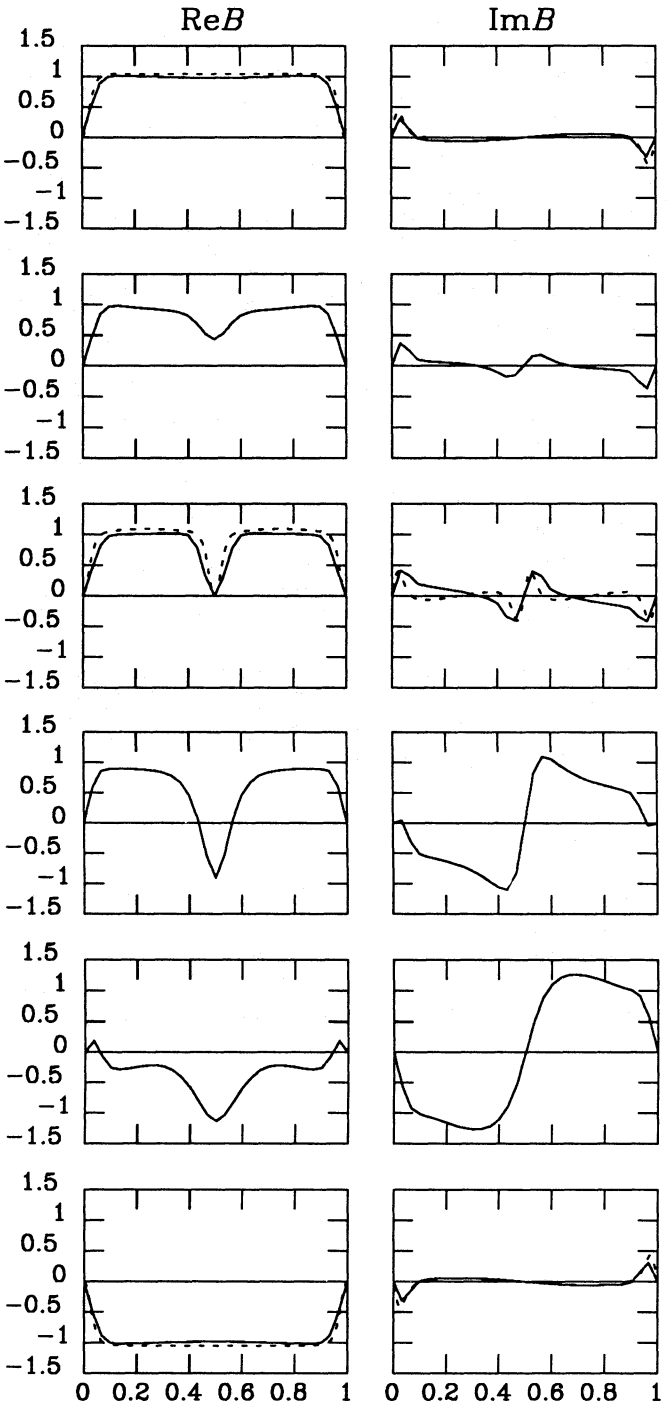

Fig. 8. Snapshots showing the magnetic field evolution during one reversal for model (ii) with stochastic forcing for $\kappa = 4$ and $C = 50$. Also displayed are with broken lines the first and second steady solution. Note the close similarity between the steady solutions and the oscillatory one at certain instants

4. Relevance to astrophysical dynamos

α^2-dynamos with isotropic α-effect exhibit usually (but not always, see Rädler & Bräuer, 1987) *steady* marginal solutions. In the nonlinear regime oscillatory solutions are possible that do not have kinematic counterparts. In our case such a solution exists already at eight times the supercritical dynamo number if the degree of nonlinearity is sufficiently strong (e.g. $\kappa = 4$). Although the oscillatory solution does not exist for smaller dynamo numbers, the steady solution is already quite sensitive to external perturbations. Small disturbances can cause field reversals. Here we want to discuss our results in the context of astrophysical dynamos.

Late-type stars can be almost fully convective. The α-effect in these stars can be very strong and the dynamo in these objects may operate then in a highly supercritical regime. Our present investigations of highly supercritical dynamos can be therefore of interest for such objects. The existence of magnetic cycles has been established for many late-type stars (Baliunas & Vaughan, 1985). It is widely believed that magnetic cycles occur as a result of $\alpha\omega$-dynamo action (e.g. Durney & Robinson, 1982). This can be justified partly because $\alpha\omega$-dynamos typically possess oscillatory solutions – in contrast to many α^2-dynamos. In addition, in the case of the Sun $\alpha\omega$-dynamos can easily produce the solar magnetic field geometry (cf. butterfly diagram, phase relation, and polar field reversals). However, the $\alpha\omega$-mechanism is not the only one to explain stellar magnetic cycles. Oscillatory solutions of highly supercritical dynamos, as discussed in the present paper, can also provide a possible mechanism for stellar magnetic cycles. This alternative to $\alpha\omega$-dynamos is interesting, because the differential rotation (ω-effect) is not necessarily strong enough in certain active stars.

There is a further argument against the $\alpha\omega$-mechanism in stars with magnetic cycles: many active stars are known which

© European Southern Observatory • Provided by the NASA Astrophysics Data System

1990A&A...238..369M

show a rotational modulation in their light curves. This suggests the existence of non-axisymmetic structures (e.g. Jetsu et al., 1990), which can be mapped in some cases explicitly by means of Doppler imaging (e.g. Piskunov et al., 1990). Non-axisymmetic structures are incompatible with strong differential rotation, because it would lead to strong dissipation due to winding up of field lines (Rädler, 1986). Thus, highly nonlinear α^2-dynamos may provide a possible mechanism for explaining magnetic cycles together with non-axisymmetric field configurations. Of course, the argument that non-axisymmetry is incompatible with large differential rotation may also loose its validity in the far nonlinear regime (Jennings et al., 1990).

The irregular solutions found in Sect. 3.5 may be of interest for explaining non-periodic activity behaviour observed for young and very active stars. Also the solar activity cycle is not exactly periodic and deviations from perfect phase stability can occur. The striking similarity between our irregular solutions (e.g. upper panel of Fig. 7) and paleomagnetic records of the Earth's magnetic field (cf. Cox, 1968) may give rise to some speculations. The basic ingredients of the reversals found in our one-dimensional model are noise and a sufficiently steep nonlinearity for which only weakly stable stationary solutions exist.

More realistic two and three-dimensional models are needed to make more precise conclusions concerning the relevance of highly supercritical dynamos to astrophysical objects such as the Sun, late-type stars, and the Earth.

References

Baliunas, S. L., Vaughan, A. H.: 1985, *Ann. Rev. Astron. Astrophys.* **23**, 379

Baryshnikova, Y., Shukurov, A.: 1987, *Astron. Nachr.* **308**, 89

Belvedere, G., Proctor, M. R. E.: 1990, in *Solar Photosphere: Structure, Convection and Magnetic Fields*, IAU Symposium No. 138, ed. J. O. Stenflo, Kluwer Acad. Publ., Dordrecht, (in press)

Brandenburg, A., Krause, F., Meinel, R., Moss, D., Tuominen, I.: 1989, *Astron. Astrophys.* **213**, 411

Cox, A.: 1968, *J. Geophys. Res.* **73**, 3247

Durney, B. R., Robinson, R. D.: 1982, *Astrophys. J.* **253**, 290

Hoyng, P.: 1988, *Astrophys. J.* **332**, 857

Jennings, R.: 1989, *Stellar Convection and Dynamo Theory*, Ph. D. thesis, University of Newcastle

Jennings, R., Weiss, N.O.: 1990, in *Solar Photosphere: Structure, Convection and Magnetic Fields*, ed. J. O. Stenflo, Kluwer Acad. Publ., Dordrecht, p. 355

Jennings, R., Brandenburg, A., Moss, D., Tuominen, I.: 1990, *Astron. Astrophys.* (in press)

Jepps, S. A.: 1975, *J. Fluid Mech.* **67**, 625

Jetsu, L., Huovelin, J., Tuominen, I., Vilhu, O., Bopp, B. W., Piirola, V.: 1990, *Astron. Astrophys.* (in press)

Krause, F., Rädler, K.-H.: 1980, *Mean-Field Magnetohydrodynamics and Dynamo Theory*, Akademie-Verlag, Berlin

Krause, F., Meinel, R.: 1988, *Geophys. Astrophys. Fluid Dyn.* **43**, 95

Lorenz, E. N.: 1963, *J. Atmosph. Sci.* **20**, 130; **20**, 448

Piskunov, N. E., Tuominen, I., Vilhu, O.: 1989, *Astron. Astrophys.* (in press)

Rädler, K.-H.: 1986, *Plasma Physics*, ESA SP-251, 569

Rädler, K.-H., Bräuer, H.-J.: 1987, *Astron. Nachr.* **308**, 101

Rüdiger, G.: 1973, *Astron. Nachr.* **294**, 183

Schmitt, D., Schüssler, M.: 1989, *Astron. Astrophys.* **223**, 343

Sokoloff, D. D., Ruzmaikin, A. A., Shukurov, A. M.: 1983, *Geophys. Astrophys. Fluid Dyn.* **25**, 293

Stix, M.: 1972, *Astron. Astrophys.* **20**, 9

Yoshimura, H.: 1978, *Astrophys. J.* **226**, 706

This article was processed by the author using Springer-Verlag TEX AA macro package 1989.

© European Southern Observatory • Provided by the NASA Astrophysics Data System